An experimental investigation on the mechanical properties of the interface between large-sized graphene and a flexible substrate

Chaochen Xu, Tao Xue, Jiangang Guo, Qinghua Qin, Sen Wu, Haibin Song, and Haimei Xie

Citation: Journal of Applied Physics **117**, 164301 (2015); doi: 10.1063/1.4918899
View online: http://dx.doi.org/10.1063/1.4918899
View Table of Contents: http://scitation.aip.org/content/aip/journal/jap/117/16?ver=pdfcov
Published by the AIP Publishing

An experimental investigation on the mechanical properties of the interface between large-sized graphene and a flexible substrate

Chaochen Xu,[1] Tao Xue,[2] Jiangang Guo,[1,a)] Qinghua Qin,[3] Sen Wu,[4] Haibin Song,[1] and Haimei Xie[1]

[1]*Tianjin Key Laboratory of Modern Engineering Mechanics, School of Mechanical Engineering, Tianjin University, Tianjin 300072, People's Republic of China*
[2]*Center for Analysis and Test, Tianjin University, Tianjin 300072, People's Republic of China*
[3]*Research School of Engineering, Australian National University, Acton, ACT 2601, Australia*
[4]*Key Lab of Precision Measurement Technology and Instruments, School of Precision Instrument and Opto-electronics Engineering, Tianjin University, Tianjin 300072, People's Republic of China*

(Received 25 January 2015; accepted 13 April 2015; published online 22 April 2015)

In this paper, the interfacial mechanical properties of large-sized monolayer graphene attached to a flexible polyethylene terephthalate (PET) substrate are investigated. Using a micro-tensile test and Raman spectroscopy, *in situ* measurements are taken to obtain the full-field deformation of graphene subjected to a uniaxial tensile loading and unloading cycle. The results of the full-field deformation are subsequently used to identify the status of the interface between the graphene and the substrate as one of perfect adhesion, one showing slide or partial debonding, and one that is fully debonded. The interfacial stress/strain transfer and the evolution of the interface from one status to another during the loading and unloading processes are discussed and the mechanical parameters, such as interfacial strength and interfacial shear strength, are obtained quantitatively demonstrating a relatively weak interface between large-sized graphene and PET. © *2015 AIP Publishing LLC*. [http://dx.doi.org/10.1063/1.4918899]

I. INTRODUCTION

Monolayer graphene of a large size produced by chemical vapor deposition (CVD) is promising as a core material for next-generation flexible electronics, battery electrodes, and optical sensors owing to its excellent mechanical and electronic transport properties.[1–4] To achieve low-cost preparation and specified functionalization of graphene, it is of critical importance to fully understand the mechanical properties and interfacial performance of graphene materials.

During the last decade, significant progress has been made in theoretical analysis, computer simulation, and experimental investigation to characterize the mechanical and interfacial properties of graphene materials. Lee *et al*. have measured the elastic properties of free-standing monolayer graphene membranes using nano-indentation together with atomic force microscopy (AFM) and have obtained a value for the Young's modulus of monolayer graphene of $E = 1.0 \pm 0.1$ TPa, which is identical to that of monolayer graphene produced by the CVD method.[5,6] Rassin *et al*., on the other hand, have studied the grain boundaries and defects induced in graphene sheets during CVD growth using molecular dynamics simulations and a first principles approach, wherein the Young's modulus of monolayer graphene was calculated as $E = 0.8$ TPa in their report.[7] Also, Guo *et al*. have studied the influence of size, chirality, and defects upon the elastic properties of monolayer and multilayer graphene using a finite element method.[8,9]

The accurate experimental measurement of the mechanical properties and behaviors of low-dimensional materials constitutes a new challenge. Recently, several new testing methods have been reported for measuring mechanical properties on the microscale. For example, synchrotron radiation X-ray computed tomography has been used to measure the microstructure evolution of ceramic materials,[10,11] *in situ* Raman spectroscopy has been employed in research on carbon nanotubes and porous silicon,[12–15] and a probe technique has explored the mechanical properties of micro/nanoscale materials.[16,17] Research based upon these new testing methods has been conducted to experimentally probe the interfacial performance of graphene. Young *et al*. have used Raman spectroscopy to monitor stress transfer in a model composite consisting of a mechanically cleaved single graphene monolayer sandwiched between two thin layers of a polymer matrix, where they found that the maximum strain that can be transferred to graphene is 0.4%, and the interfacial shear strength was found to be 0.5 and 0.25 MPa after fragmentation.[18,19] Jiang *et al*. have researched the nonlinear mechanical response of monolayer graphene on polyethylene terephthalate (PET) using *in situ* Raman spectroscopy and AFM and have found that the maximum strain ranges from 1.2% to 1.6% and interfacial shear strength ranges between 0.46 and 0.69 MPa.[20] Using AFM, Mario *et al*. have analyzed the morphology and performance of graphene to adapt to rough substrates and have found that the roughness decreased the adhesion between the graphene and the substrate.[21]

Table I tabulates the results for the interfacial adhesion energy of monolayer graphene found by these previous works using theoretical models, simulation methods, or

a)Author to whom correspondence should be addressed. Electronic mail: guojg@tju.edu.cn

TABLE I. Interfacial adhesion energy of graphene on different substrates.

Reference number	Research method	Size and type of graphene	Type of substrate	Adhesion energy (mJ/m^2)
22	Theoretical model	…	h-BN	367
23	Theoretical model	…	PDMS[a]	3.5–7.4
24	Atomistic simulation	…	Graphene	400
25	SEM experiment	WMCN[b]	Graphene	200–360
26	AFM experiment	ME[c]/5 μm	SiO_2	450
27	AFM experiment	ME/10–20 μm	Au/Cu	176[d]
28	AFM experiment	ME/10–20 μm	PDMS	7.04[d]

[a]PDMS stands for polydimethylsiloxane, and is a kind of plastic.
[b]WMCN stands for multiwalled carbon nanotube.
[c]ME stands for mechanical exfoliation.
[d]Unit used in Refs. 27 and 28 (eV/nm^2).

experiments, where it can be seen that the interfacial performance of graphene as concluded from these previous works varies greatly. The variation of the adhesion energy or interfacial shear strength extracted by different theoretical or experimental methods is almost two orders of magnitude, suggesting that the interfacial properties of graphene can be influenced by many factors, which makes this a particularly complex mechanical problem. Up to now, the theoretical analysis has been based upon the simulations and predictions of a mechanical model considering the influence of several factors, while the experimental studies have mainly focused upon mechanically cleaved graphene samples that are fairly small in size, ranging from a few to dozens of microns. However, the interfacial performance of large-sized graphene is much more susceptible than small-sized graphene to various factors, such as the types of graphene, the defect level, the substrate material and its surface roughness, and especially the size effect. Therefore, it is necessary to carry out experimental measurements and systematically analyze the interfacial properties of large-sized graphene.

In this paper, we focus on a large-sized monolayer of graphene produced by CVD, and investigate the mechanical properties of the interface between the large-sized graphene and the PET substrate in the tangential direction. With *in situ* Raman spectroscopy measuring the whole-field deformation of graphene that is subjected to a uniaxial tensile loading and unloading cycle, the process of interfacial stress/strain transfer from the PET surface to the graphene is analyzed and the evolution of the bonding state existing at the interface during loading and unloading is discussed. The mechanical parameters of the interface, such as the strength, stiffness, and shear strength, are also provided.

II. LARGE-SIZED GRAPHENE/PET SPECIMEN AND RAMAN EXPERIMENT

The schematic diagram of the experimental setup is shown in Fig. 1(a), including a micro-Raman system and a large-sized monolayer graphene/PET specimen. The large-sized monolayer graphene samples used here are synthesized by CVD with dimensions of 10-mm long by 3-mm wide. The size of the PET substrate is 20-mm long, 3-mm wide, and 0.1-mm thick. PET is a flexible substrate with a large deformation, as shown by its stress–strain curve depicted in Fig. 1(b), in which the elastic region ranges from 0% to 3%. The stress-strain curve for PET is measured by an

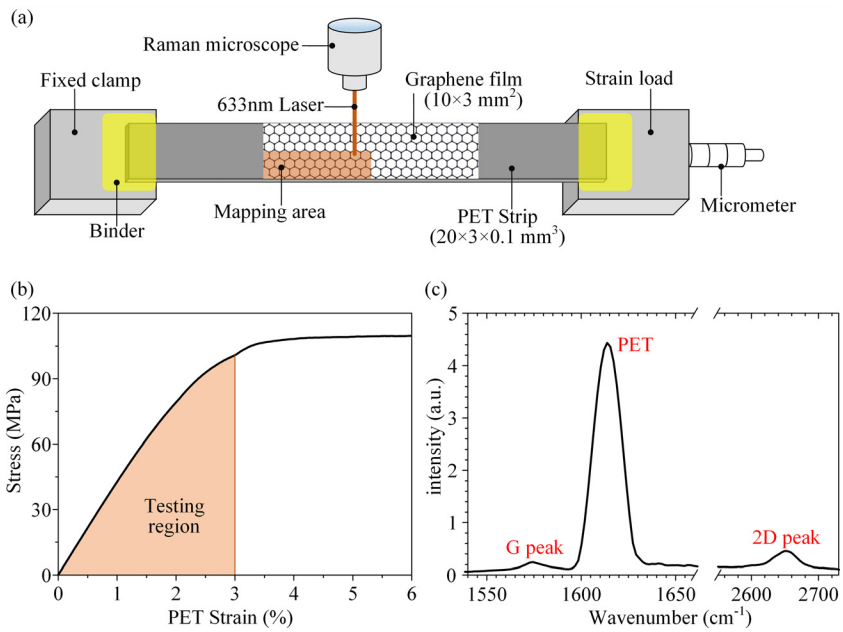

FIG. 1. (a) Schematic diagram of the experimental setup (micro-Raman system and graphene/PET specimen, not to scale). (b) Stress–strain curve of PET by uniaxial tension test. (c) Raman spectrum of graphene on PET before loading (the characteristic peak at 1615 cm^{-1} is from the PET background).

Instron3343P1018 universal tensile testing machine. The monolayer graphene film is easily transferred by a chemical method to the top surface of the PET substrate with minimal holes or cracks (<5% of the film area).[29] After transfer, the graphene sheet can be attached to the PET substrate by Van der Waals forces. The graphene/PET specimen is subjected to a uniaxial tensile loading and unloading schedule by an ingenious micro-loading device with a minimum step of 10 μm. The substrate is stretched from 0% up to the maximum strain 3% to guarantee that the whole process will proceed in the elastic region of PET. The loading step is set to be 10 μm (0.05% strain), which is small to ensure the strain to be uniform along the PET, while the unloading step is set to be 50 μm (0.25% strain).

In situ Raman spectroscopy is employed to measure the whole field strain distribution of graphene during the loading and unloading process because of its advantages of being non-contact and non-destructive and having high spatial resolution.[30] The basic principle of the Raman-based stress measurement theories is that the spectral information from Raman scattering is related to the lattice vibrations (phonons) of the material to be tested, and once deformed, the wavenumber (also called as Raman frequency) of the characteristic peaks of this specific material in the spectrum will shift. The characteristic G and 2D Raman bands of monolayer graphene will shift to lower or higher positions under tensile or compressive load, and the relationship between the Raman band-shifts and the strain in graphene can be determined by Grüneisen parameters.[31] The shift of the 2D Raman band is traced to measure the strain in graphene because of its extreme sensitivity to strain. Figure 1(c) is the Raman spectrum of the monolayer graphene on PET before loading, showing the characteristic intensities and waveforms of monolayer graphene, and the initial position of the 2D Raman band is 2651 cm^{-1}. The well-defined Raman spectra are obtained through a Renishaw InVia system with a 633 nm and 0.23 mW He-Ne laser as the excitation source. The spot size of the laser is approximately 1.2 μm in diameter, focused through a 50× objective lens.

III. MEASUREMENT AND ANALYSIS OF THE INTERFACIAL STRAIN TRANSFER

The Raman mapping method is used to scan the whole-field distribution of the 2D-Raman band position of graphene during a loading–unloading process. Considering the symmetry of the specimen, the mapping area (5000 × 1500 μm^2) is a quarter of the entire graphene area, which can be seen as the shaded region in Fig. 2(c). The parameters set for Raman mapping are a horizontal step length of 50 μm, a vertical step length of 75 μm, a Raman scanning center of 2000 cm^{-1} (Raman band position), and a scanning time of 10 s. Similar mapping in small-sized graphene has been undertaken in a previous paper.[4] Figure 2(a) shows the contour maps of the 2D-Raman band position of the monolayer graphene at different levels of PET tensile strain applied in the horizontal direction, where information on the zero-strain state for graphene can be obtained from the contour map at a PET strain of 0%. Before loading, the main part of the region of graphene is yellow, representing the initial position of the 2D-Raman band at 2651 cm^{-1}, excepting some individual regions of orange, representing the position around 2654 cm^{-1}. This relatively high position of the 2D-Raman band indicates that a minor local compressive strain is induced in several regions of the graphene during the chemical transfer process.

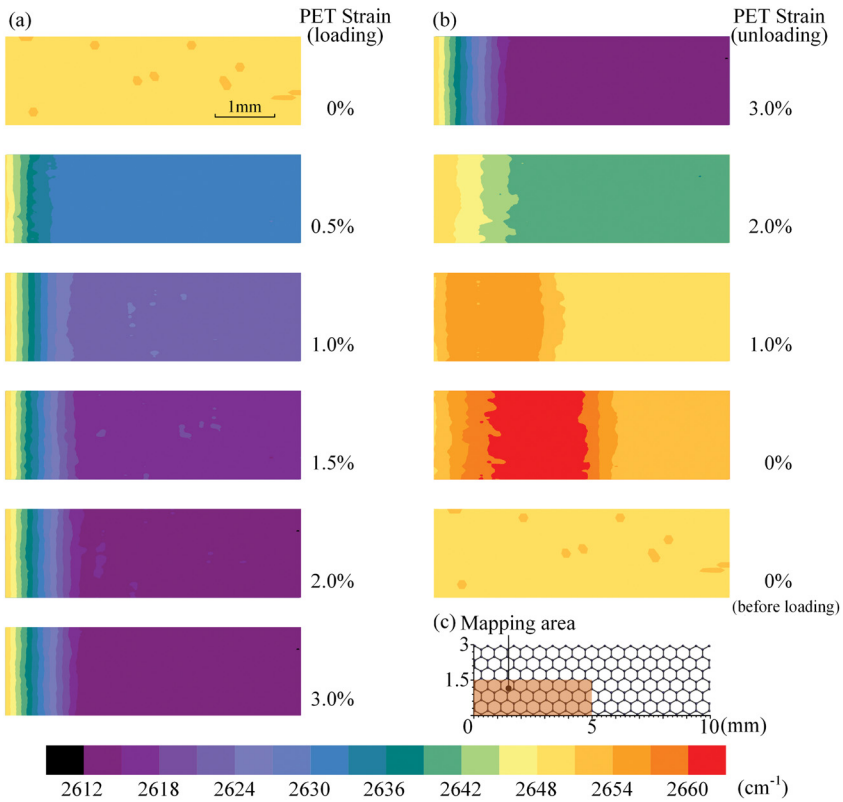

FIG. 2. Contour maps of the 2D-Raman band position of the monolayer graphene at different levels of PET tensile strain applied in the horizontal direction for (a) loading and (b) unloading (the last contour map placed here is the 2D-Raman band distribution before loading for comparison with the distribution after complete releasing). The bar legend (bottom) plots the relationship between the contour colors and the position of the 2D-Raman band (cm^{-1}). (c) Schematic plot showing the mapping area (shaded) in relation to the size of the graphene area.

However, the 2D-Raman band of these regions is only 3 cm^{-1} higher than the position of most regions, which is small enough to be neglected. The position of the 2D-Raman band of the monolayer graphene in the vertical direction is uniform at each level of strain. Hence, the effect of the sides upon the deformation caused by the edges of the graphene can be ignored. However, the position of the 2D-Raman band in the horizontal direction is not uniform at each level of strain after loading, but instead the colors gradually vary from the edge until they stabilize in the central region. The 2D-Raman band/strain gradient region existing on the margin of the graphene suggests the existence of a non-uniform tensile deformation, and the length of the region is gradually varied at each level of strain. Apart from these strain gradient regions, the 2D-Raman band of most of the graphene in the central area remains nearly constant. As the substrate stretches from 0% to 3%, the position of the 2D-Raman band reduces by 37 cm^{-1}, exhibiting a red shift to 2614 cm^{-1} from the zero-strain state of 2651 cm^{-1}. Using the same approach, the contour maps of the 2D-Raman band position of the monolayer graphene at different levels of PET strain during unloading are plotted in Fig. 2(b). Similar to the behavior seen in the loading process, a 2D-Raman band/strain gradient region also exists on the margin at each level of the unloading strain, illustrating that the deformation of graphene is not uniform in this process. When the substrate is released from 3% to 0%, the position of the 2D-Raman band gradually recovers from 2614 cm^{-1} to the zero-strain state of 2651 cm^{-1} and then continues to blue shift to 2660 cm^{-1} (red color in Fig. 2(b)). This means that the compressive strain appears through the graphene and can be distinguished by comparing the contour maps recorded before stretching and after complete release (Fig. 2(b)).

The contour maps of the Raman experiment in Fig. 2 show the non-uniform strain distribution of the graphene along the direction of the tensile axis as the strain of the PET substrate increases uniformly. This is because the bonding state of the interface between the large-sized graphene and the PET is not the same in every region, and the strain of the substrate in some regions cannot be perfectly transferred to the overlaying graphene. To study the bonding state of the interface, the central point of the graphene is chosen as an observation spot first, probing the strain of this region versus the PET strain. Figure 3(a) depicts the evolution of the 2D-Raman band of graphene at the central point with increasing PET strain. It can be clearly determined that the position of the 2D-Raman band starts to red shift linearly from the initial 2651 cm^{-1} position at a rate of -36 cm^{-1} per % until approximately 2633 cm^{-1}, which corresponds to the applied PET strain of 0.5%, and then continues to red shift to 2614 cm^{-1}. The rate of -36 cm^{-1} per % can now be used to convert the Raman band shift to graphene strain. When the PET is stretched up to 3%, the process of graphene strain can be divided into three stages called the linear stage, the non-linear stage, and the stable stage, where the demarcation points between these three stages are the PET strain values of 0.5% and 2%. In the first (linear) stage, the graphene strain equals the PET strain, which means that the deformation in the substrate completely transfers to the graphene on its surface, while the graphene tightly adheres to the PET by the Van der Waals force. In the second (nonlinear) stage, the graphene strain is less than the PET strain, which means that only part of the deformation in the substrate is transferred. At this point, interfacial slide begins between the graphene and PET because the Van der Waals force is not strong enough to keep them together. In the third (stable) stage, the graphene strain does not change even as the PET strain keeps increasing, which means that the deformation in the substrate is not transferred and that the graphene and PET totally debond in the tangential direction. Therefore, by comparing the relative strains of the graphene ($\Delta\varepsilon_g$) and the PET substrate ($\Delta\varepsilon_s$), the bonding states of the interface between them can be classified into the three stages of interfacial adhesion ($\Delta\varepsilon_g = \Delta\varepsilon_s$), interfacial slide in the tangential direction ($\Delta\varepsilon_g < \Delta\varepsilon_s$), and interfacial debonding in the tangential direction ($\Delta\varepsilon_g = 0$) or, in short, adhesion, slide, and debonding. The shaded regions in the strain-strain plot for the graphene

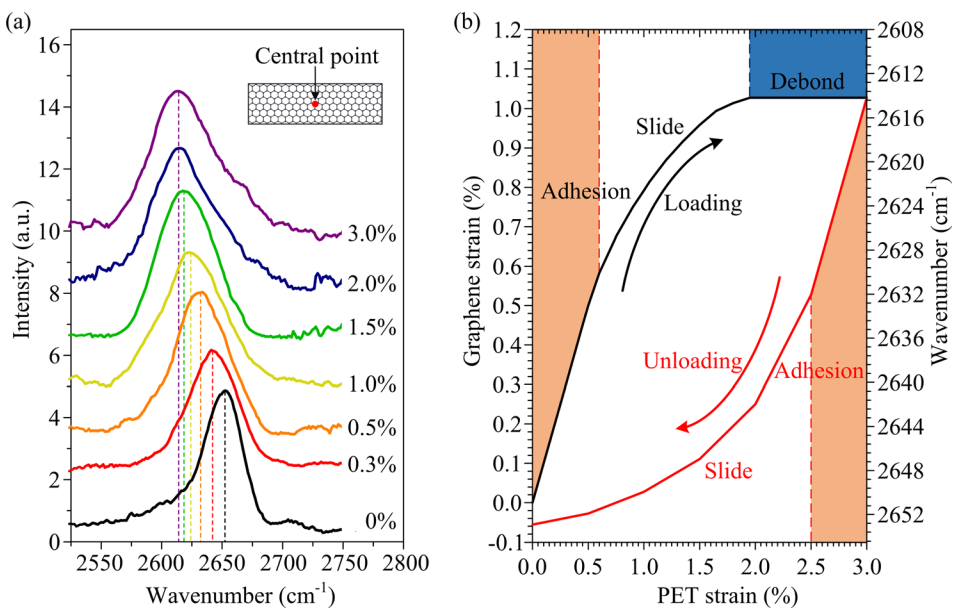

FIG. 3. (a) The 2D-Raman band of graphene at the central point for different PET strain values. (b) The 2D-Raman band/strain in graphene as a function of PET strain during the loading (black) and unloading (red) process. The shaded regions in (b) indicate the adhesion (red), slide (white) and debonding (blue) stages.

and PET in Fig. 3(b) mark the three bonding states, wherein the critical PET strain for adhesion during loading is 0.5% and the ultimate strain before debonding is 2%. The same analytical method is used for the unloading process, and plots the position of the 2D-Raman band/strain in graphene as a function of PET strain in Fig. 3(b). At the initial unloading PET strain of 0.5% (from 3% to 2.5%), the graphene adheres to the substrate and the decrement of graphene strain is equal to that of the PET strain until they decrease together by 0.5%. At this stage of the unloading, the linear elastic-like deformation of 0.5% during the loading process is recovered immediately at the beginning of the unloading process. After the critical strain for adhesion, interfacial sliding is then seen to occur between graphene and PET, but the debonding state does not appear at the central point of the graphene throughout the entire unloading process.

To understand the interfacial transfer of strain between the graphene and substrate that exists throughout the whole large-sized graphene, Figure 4(a) shows the variation of the graphene strain along the centerline of the monolayer during the loading process for 15 values of PET tensile strain up to 3%, with a strain value increment of 0.15%. It is clear that

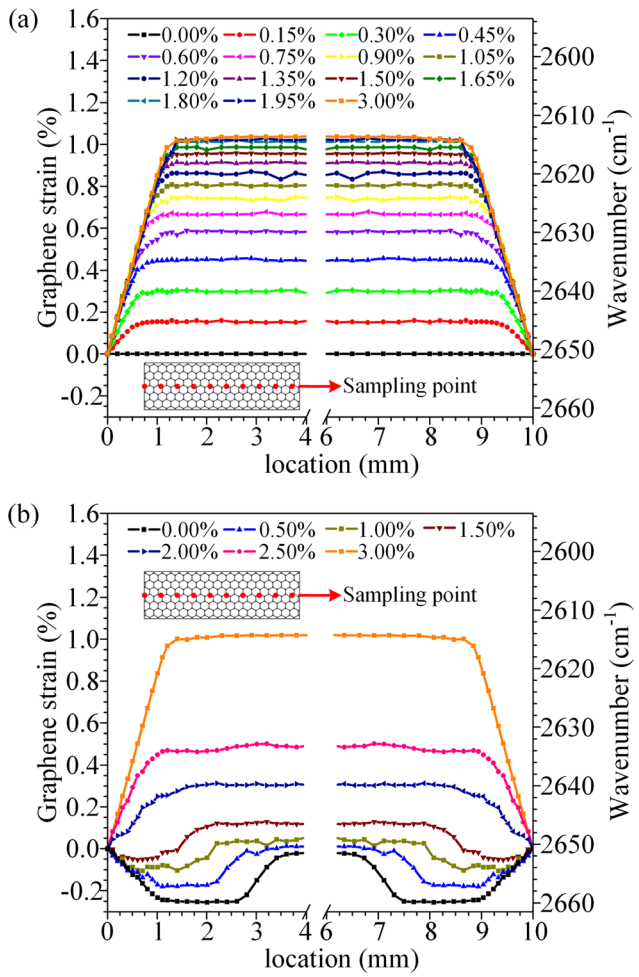

FIG. 4. Variation of the graphene strain along the centerline of the monolayer for PET tensile strains of 0%–3% during the (a) loading and (b) unloading process. (Inset) Schematic showing the locations of the sampling points across the graphene monolayer (the data for locations 1–5 mm are measured and the values of the data for locations 5–10 mm are symmetric).

the maximum strain that can be transferred from the PET to the graphene is 1.03%, which can be considered the limit strength of graphene in the tangential direction. The strain gradient region existing on the margin of graphene can be easily distinguished at each level of PET strain, and the relative length of this region and its plateau gradually changes over the loading process. The length of the strain gradient region in which the graphene strain rises from 0% to approximately 90% of the plateau value is defined as the "critical length," l_c, and the ratio of the critical length to total length (l/l_c) can represent the quality of the interface between the graphene and the substrate. In other words, a larger ratio corresponds to a stronger interface.[32] As the graphene/PET system stretches, the critical length increases from 1000 to 2200 μm and the ratio decreases from 10 to 4.55, suggesting that the combination of the interface becomes weaker during the loading process. Similarly, Figure 4(b) shows the variation of the graphene strain along the centerline of the monolayer over the unloading process at seven values of PET strain, with a strain decrement of 0.5%. Compressive strain appears in the margin of the graphene when the PET strain relaxes back to 1.5%, and the area of compressive strain gradually expands from the margin to the center with further unloading until, finally, the whole graphene overlayer is under compression with a maximum compressive strain of −0.26% when the PET is completely relaxed to 0%. The critical length further increases from 2200 to 3500 μm and the ratio decreases to 1.43, suggesting that the combination of the interface further weakens during the unloading process.

To further explore the bonding states of the interface in every region of the entire large-sized graphene flake, a difference analysis is conducted by calculating the difference in the strain value of the graphene between every two adjacent curves ($\Delta\varepsilon_g$) in Fig. 4(a) and then compare it with the constant substrate strain increment ($\Delta\varepsilon_s = 0.15\%$). As was determined earlier by the bonding state defined in the analysis of the central point of the graphene, if $\Delta\varepsilon_g = \Delta\varepsilon_s = 0.15\%$, this region is in an adhesion state. If, however, $\Delta\varepsilon_g < \Delta\varepsilon_s = 0.15\%$, this region is in the slide state; and if $\Delta\varepsilon_g = 0$, this region is in the debonding state. Figure 5 gives the result of the difference analysis (showing only the left part of graphene, with the right part being symmetric). When the PET strain is less than 0.5%, the entire graphene flake, except for the margin, is in the adhesion bonding state, and the strain can be completely transferred from PET to graphene. With increasing PET strain, the slide state region at the margin equally extends from 0 μm to the position at approximately 1600 μm, until it suddenly extends to the center after the PET strain value surpasses 0.5%. Therefore, the PET strain of 0.5% is the critical point between the adhesion and slide states, beyond which the whole graphene slides and only a portion of the strain can be transferred. When the PET strain is more than 0.75%, the debonding region appears and equally expands from the edge at 0 μm to the position at approximately 900 μm with increasing PET strain, until it suddenly extends to the center after the PET strain value exceeds 2%. Therefore, a PET strain of 2% is the critical point between the slide and debonding states, beyond which the whole graphene debonds and no strain can be transferred. The extension of the slide region and the

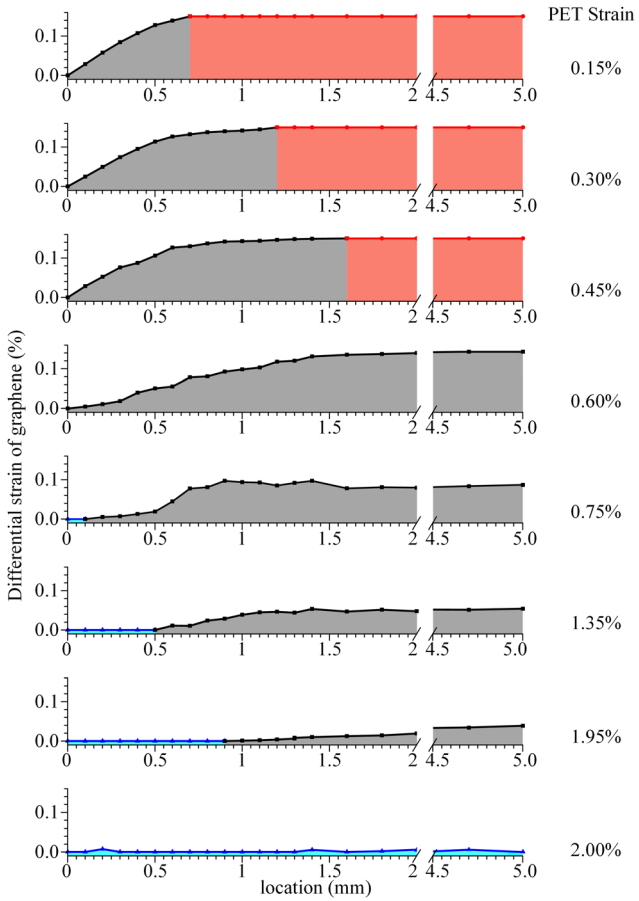

FIG. 5. Plot of the difference in the strain value of the graphene between every two adjacent curves ($\Delta\varepsilon_g$) in Fig. 4(a) (eight levels of strain are shown), showing the regions in the graphene exhibiting the adhesion state where $\Delta\varepsilon_g = 0.15\%$ (red shading), the slide state where $\Delta\varepsilon_g < 0.15\%$ (grey shading), and the debonding state where $\Delta\varepsilon_g = 0$ (blue shading).

debonding region is similar owing to the existence of the critical points. This phenomenon should be seriously considered because interfacial failure occurs instantaneously once beyond the critical point, and thus it is imperative that the limit deformation of device substrates is controlled. The same analysis is applied to the unloading process, and the bonding state of the interface in every region of the entire large-sized graphene flake is obtained. During the initial part of the unloading process wherein the PET strain is reduced by 0.5%, the entire graphene flake except for the margin adheres to the substrate. After the critical strain for adhesion is reached, the interfacial slide occurs throughout the entire graphene flake. No debonding state appears in any region of graphene until the substrate relaxes to 0%. In a manner similar to the situation of the graphene central point, the linear elastic-like deformation of 0.5% over the loading is recovered immediately in the beginning of the unloading process in the adhesion state region.

IV. ANALYSIS OF THE INTERFACIAL MECHANICS OF GRAPHENE

Now, the interfacial stress transfer between the large-sized graphene and the substrate is explored based on the force analysis of an element of graphene. Using a force balance[17,33] of the shear forces at the interface and the tensile forces in a flake element, as shown in Fig. 5(a), the relationship between the interfacial shear stress, τ, and the normal stress, σ, can be determined as

$$\frac{d\sigma}{dx} = -\eta\frac{\tau}{t}, \tag{1}$$

$$\tau = -\frac{Et}{\eta}\frac{d\varepsilon}{dx}, \tag{2}$$

where ε is the normal strain in graphene, E is the Young's modulus, t is the thickness of the graphene, and η is the effective contact rate between the graphene and the PET. In this paper, we take $E = 1$ TPa as the Young's modulus of graphene, $t = 1$ nm as the thickness of the CVD graphene provided by manufacturer, and $\eta = 0.7$ based upon previous papers[20,34] and discussed below. The force owing to the shear stress at the interface, τ, is balanced by the force owing to the variation of the normal stress in the graphene, $d\sigma$, which is deduced from the force balance equation given in Eq. (1). Therefore, taking the derivative of the smoothed graphene strain curves in Fig. 4 and then multiplying by the related constant coefficients representing the properties of graphene, the interfacial shear stress throughout the graphene can be obtained. The strain variation and interfacial shear stress along the centerline of the graphene at a PET strain of 0.5% (Fig. 6(b)) and 1.5% (Fig. 6(c)) are shown. The bonding state of the interface can also be judged by the interfacial stress, as illustrated in Fig. 6(a). In the adhesion state, the interfacial stress, τ, equals zero, indicating the common deformation of graphene and substrate. The interfacial sliding begins when τ is increased beyond zero and, when the interfacial shear stress reaches a critical value, interfacial debonding occurs between the graphene and the substrate. This critical value for debonding is inherent and varies in terms of the different interfaces between two specific materials, where the critical shear stress between large-sized graphene and the PET substrate here is 0.012 MPa. Figure 6(b) plots the normal and interfacial shear stress at a PET strain value of 0.5%, where it can be seen that the central region of graphene is in the bonding state of adhesion, and the slide region in the margin has extended to a position at approximately 1700 μm. At a PET strain value of 1.5% (Fig. 6(c)), the slide region extends to include the entire center, and the debonding region appears and expands from the edge of the graphene to approximately 600 μm into the flake. The bonding state of the interface judged by the interfacial stress in Fig. 6 is identical to that judged by the difference analysis in Fig. 5.

V. CONCLUSIONS AND DISCUSSION

In this paper, the *in situ* Raman spectroscopy technique is employed to investigate the mechanical properties of the tangential interface between the flexible PET substrate and the larde-sized graphene through the Van der Waals force. The process of interfacial stress transfer from the PET to the graphene is analyzed and some new experimental phenomena are observed where, in particular, three states indicating adhesion, slide, and debonding of the graphene-substrate structure are studied. It is found that the critical strain that determines the end of the adhesion state is equal to a PET strain of 0.5%,

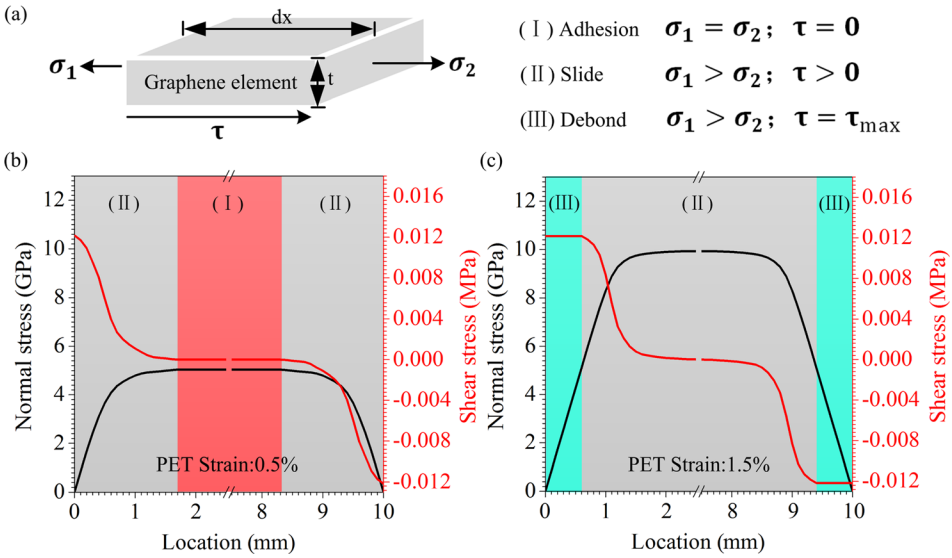

FIG. 6. (a) Schematic of the graphene element illustrating the bonding state of the interface as a function of the interfacial stress. (b) and (c) Plots of the strain variation (black) and interfacial shear stress (red) along the centerline of the graphene at a PET strain of (b) 0.5% and (c) 1.5% showing the adhesion region (red shading), the slide region (grey shading), and the debonding region (blue shading).

and the critical strain for the onset of tangential debonding is equal to a PET strain of 2%. The maximum strain that can be transferred to graphene is 1.02%, which is similar to the value found in the works of Jiang *et al.* and Young *et al.*[18–20] However, the maximum interfacial shear strength is found to be 0.012 MPa, which is one order of magnitude smaller than that reported in the literature. To explain this relatively small value, several possible explanations are provided.

(1) It is possible that there exists an imperfect contact between the graphene and substrate. A topographic AFM scan of the PET substrate in an area of $20 \times 20\ \mu m^2$ in Fig. 7 shows the undulation of the PET surface, implying that it is not a perfectly smooth plane in the nanoscale. The cross-section of a topographic AFM map in a relatively smooth area (I) shows that the average height of the PET surface undulation is 5 nm, and the height of the undulation in the most rough areas (II) is up to 30 nm. The relatively smooth area accounts for approximately 70% of the entire surface area, so the coefficient $\eta = 0.7$ representing the effective contact rate between the graphene and PET is introduced in the force balance equation to partially modify the influence of the roughness.[34]

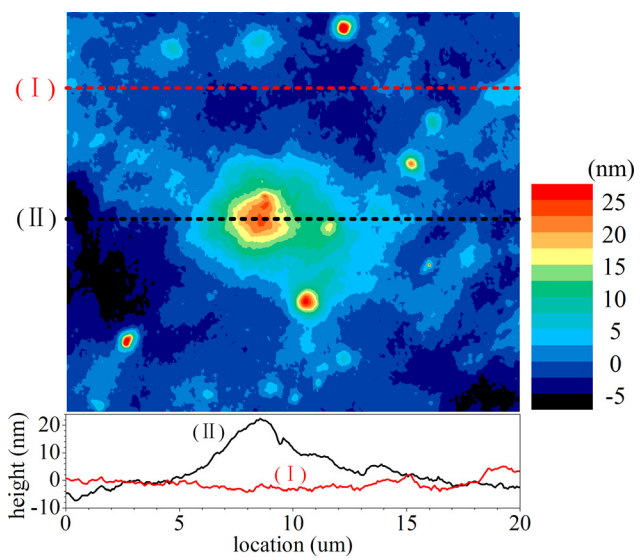

FIG. 7. Atomic force microscope scan of the PET substrate in an area $20 \times 20\ \mu m^2$ (obtained by Bruker Dimension ICON Nanoscope V). The bar legend (right) plots the relationship between the contour colors and the topographic surface height (nm). The cross-section of the topographic AFM map taken in a relatively smooth area (I) and in a rough area (II) is plotted below.

(2) The material properties of the graphene produced by CVD and of the plastic PET substrate are different from those assumed in previous theoretical models and those that existed in previous experimental studies. The interface between the CVD graphene and the PET comprises only the Van der Waals force without any adhesives or glues. Previous works using different theoretical or experimental methods have shown a variation of the extracted adhesion energy of almost two orders of magnitude, where the adhesion energy between graphene and a plastic material has been the smallest.[23,28] In addition, the graphene produced by the CVD method is polycrystalline, and the Young's modulus of the polycrystalline graphene produced by CVD method is lower than that produced by mechanical exfoliation because of several defects existing in the polycrystalline graphene.[7,9] As is given in Eq. (2), the interfacial shear strength is proportional to the Young's modulus, so the adhesion strength of this interface will be relatively weak compared with that of monocrystalline graphene.

(3) The last explanation for the small interfacial shear strength is the size effect. The length of the CVD graphene used in this paper is 10 000 μm, which is two or three orders of magnitude larger than that of the mechanically cleaved graphene used in previous studies. As is shown by the force-balance equation in Eq. (1), the interfacial shear stress is in direct proportion to the derivative of the slope of the strain to the length, so the maximum strain that can be transferred to graphene in this work is similar to that found from previous works conducted on micrometer-sized graphene. However, the length of the strain gradient region is different and is in proportion to the size of graphene. Therefore, the size effect will significantly influence the shear stress/strain in the interface

because the strain gradient region in millimeter-sized graphene is much larger. The size effect occurs when the size of a specimen affects its mechanical properties, so we speculate that the mechanical properties of graphene are affected by its size as well. However, the exact relationship between the size and interfacial properties of graphene calls for further research.

In summary, Raman spectroscopy is an effective means by which to study the mechanical and interfacial properties of graphene. This paper shows that the mechanical properties of the interface between large-sized graphene and a substrate are apparently affected by many factors such as the size of the graphene, the texture of the substrate material, and the roughness of substrate. Therefore, the interfacial properties and the interfacial strain transfer process of large-sized graphene need to be considered in practical applications.

ACKNOWLEDGMENTS

This work was financially supported by the National Basic Research Program of China (2012CB937500) and the National Natural Science Foundation of China (11227202 and 11272232).

[1]S. Bae, H. Kim, Y. Lee, X. Xu, J. S. Park, Y. Zheng, J. Balakrishnan, T. Lei, H. R. Kim, Y. I. Song, Y. J. Kim, K. S. Kim, B. Ozyilmaz, J. H. Ahn, B. H. Hong, and S. Iijima, Nat. Nanotechnol. **5**, 574 (2010).
[2]D. Choi, M. Y. Choi, W. M. Choi, H. J. Shin, H. K. Park, J. S. Seo, J. Park, S. M. Yoon, S. J. Chae, Y. H. Lee, S. W. Kim, J. Y. Choi, S. Y. Lee, and J. M. Kim, Adv. Mater. **22**, 2187 (2010).
[3]S. Won, Y. Hwangbo, S. K. Lee, K. S. Kim, K. S. Kim, S. M. Lee, H. J. Lee, J. H. Ahn, J. H. Kim, and S. B. Lee, Nanoscale **6**, 6057 (2014).
[4]A. P. A. Raju, A. Lewis, B. Derby, R. J. Young, I. A. Kinloch, R. Zan, and K. S. Novoselov, Adv. Funct. Mater. **24**, 2865 (2014).
[5]C. Lee, X. Wei, J. W. Kysar, and J. Hone, Science **321**, 385 (2008).
[6]G. H. Lee, R. C. Cooper, J. An, S. S. Lee, A. Zande, N. Petrone, A. G. Hammerberg, C. G. Lee, B. Crawford, W. Oliver, J. W. Kysar, and J. Hone, Science **340**, 1073 (2013).
[7]R. Grantab, V. B. Shenoy, and R. S. Ruoff, Science **330**, 946–948 (2010).
[8]S. P. Wang, J. G. Guo, and Y. Jiang, J. Comput. Theor. Nanosci. **10**, 250 (2013).
[9]S. P. Wang, J. G. Guo, and L. J. Zhou, Physica E **48**, 29 (2013).
[10]M. Wang, X. F. Hu, and X. P. Wu, Mater. Res. Bull. **41**, 1949 (2006).
[11]F. Xu, Y. Li, X. Hu, Y. Niu, J. Zhao, and Z. Zhang, Mater. Lett. **67**, 162 (2012).
[12]W. Qiu, Y. L. Kang, Z. K. Lei, Q. H. Qin, Q. Li, and Q. Wang, J. Raman. Spectrosc. **41**, 1216 (2010).
[13]Q. Li, W. Qiu, X. H. Tan, J. G. Guo, and Y. L. Kang, Opt. Laser. Eng. **48**, 1119 (2010).
[14]Y. Kang, Y. Qiu, Z. Lei, and M. Hu, Opt. Laser. Eng. **43**, 847 (2005).
[15]W. Qiu, Q. Li, Z. K. Lei, Q. H. Qin, W. L. Deng, and Y. L. Kang, Carbon **53**, 161 (2013).
[16]X. Li and Y. Peng, Appl. Phys. Lett. **89**, 234104 (2006).
[17]X. Li, D. Su, and Z. Zhang, Sens. Actuators, A **153**, 13 (2009).
[18]L. Gong, I. A. Kinloch, R. J. Young, I. Riaz, R. Jalil, and K. S. Novoselov, Adv. Mater. **22**, 2694 (2010).
[19]R. J. Young, L. Gong, I. A. Kinloch, I. Riaz, R. Jalil, and K. S. Novoselov, ACS Nano **5**, 3079 (2011).
[20]T. Jiang, R. Huang, and Y. Zhu, Adv. Funct. Mater. **24**, 396 (2014).
[21]M. Lanza, Y. Wang, H. Sun, Y. Tong, and H. Duan, Acta Mech. **225**, 1061 (2014).
[22]C. Zhang, J. Lou, and J. Song, J. Appl. Phys. **115**, 144308 (2014).
[23]Z. Zhang and T. Li, J. Appl. Phys. **110**, 083526 (2011).
[24]Z. Lu and M. L. Dunn, J. Appl. Phys. **107**, 044301 (2010).
[25]M. R. Roenbeck, X. Wei, A. M. Beese, M. Naraghi, A. O. Furmanchuk, J. T. Paci, G. C. Schatz, and H. D. Espinosa, ACS Nano **8**, 124 (2014).
[26]S. P. Koenig, N. G. Boddeti, M. L. Dunn, and J. S. Bunch, Nat. Nanotechnol. **6**, 543 (2011).
[27]S. Scharfenberg, N. Mansukhani, C. Chialvo, R. L. Weaver, and N. Mason, Appl. Phys. Lett. **100**, 021910 (2012).
[28]S. Scharfenberg, D. Z. Rocklin, C. Chialvo, R. L. Weaver, P. M. Goldbart, and N. Mason, Appl. Phys. Lett. **98**, 091908 (2011).
[29]X. Li, W. Cai, J. An, S. Kim, J. Nah, D. Yang, R. Piner, A. Velamakanni, I. Jung, E. Tutuc, S. K. Banerjee, L. Colombo, and R. S. Ruoff, Science **324**, 1312 (2009).
[30]W. Qiu and Y. L. Kang, Chin. Sci. Bull. **1**, 14 (2014).
[31]T. M. G. Mohiuddin, A. Lombardo, R. R. Nair, A. Bonetti, G. Savini, R. Jalil, N. Bonini, D. M. Basko, C. Galiotis, N. Marzari, K. S. Novoselov, A. K. Geim, and A. C. Ferrari, Phys. Rev. B **79**, 205433 (2009).
[32]A. Kelly and N. H. Macmillan, *Strong solids* (Clarendon Press, Oxford, 1986).
[33]S. Timoshenko, *Strength of Materials* (Van Nostrand Company, New York, 1930).
[34]S. V. Kusminskiy, D. K. Campbell, A. C. Neto, and F. Guinea, Phys. Rev. B **83**, 165405 (2011).